Journal of Optics

PAPER • OPEN ACCESS

Unbalanced gain and loss in a quantum photonic system

To cite this article: Charles Andrew Downing and Oliver Isaac Reuben Fox 2023 *J. Opt.* **25** 095201

View the article online for updates and enhancements.

You may also like

- A Real Expectation Value of the Time-dependent Non-Hermitian Hamiltonians
F Kecita, A Bounames and M Maamache
- A physical interpretation for the non-Hermitian Hamiltonian
L Jin and Z Song
- New topological invariants in non-Hermitian systems
Ananya Ghatak and Tanmoy Das

This content was downloaded from IP address 46.64.57.13 on 20/12/2023 at 14:38

OPEN ACCESS
IOP Publishing
Journal of Optics
J. Opt. **25** (2023) 095201 (10pp)
https://doi.org/10.1088/2040-8986/ace5be

Unbalanced gain and loss in a quantum photonic system

Charles Andrew Downing* **and Oliver Isaac Reuben Fox**

Department of Physics and Astronomy, University of Exeter, Exeter EX4 4QL, United Kingdom

E-mail: c.a.downing@exeter.ac.uk

Received 25 April 2023, revised 23 June 2023
Accepted for publication 10 July 2023
Published 25 July 2023

Abstract

Theories in physics can provide a kind of map of the physical system under investigation, showing all of the possible types of behavior which may occur. Certain points on the map are of greater significance than others, because they describe how the system responds in a useful or interesting manner. For example, the point of resonance is of particular importance when timing the pushes onto a person sat on a swing. More sophisticatedly, so-called exceptional points have been shown to be significant in optical systems harbouring both gain and loss, as typically described by non-Hermitian Hamiltonians. However, expressly quantum points of interest—be they exceptional points or otherwise—arising in quantum photonic systems have been far less studied. Here we consider a paradigmatic model: a pair of coupled qubits subjected to an unbalanced ratio of gain and loss. We mark on its map several flavours of both exceptional and critical points, each of which are associated with unconventional physical responses. In particular, we uncover the points responsible for characteristic spectral features and for the sudden loss of quantum entanglement in the steady state. Our results provide perspectives for characterizing quantum photonic systems beyond effective non-Hermitian Hamiltonians, and suggest a hierarchy of intrinsically quantum points of interest.

Supplementary material for this article is available online

Keywords: non-Hermitian Hamiltonian, exceptional points, quantum master equation, qubits, open quantum systems

(Some figures may appear in colour only in the online journal)

1. Introduction

Conventionally, quantum mechanics deals with with Hermitian Hamiltonians. This common restriction ensures both real eigenvalues and unitary time evolution. Remarkably, relaxing this constraint by employing non-Hermitian Hamiltonians can also lead to a physical quantum theory [1–3]. Most famously, constructing a quantum theory obeying the less strict condition of parity-time (or $\mathcal{PT}$) symmetry has led to some spectacular theoretical predictions within modern optics [4–7]. In particular, theoretical treatments of gain and loss naturally lead to non-Hermitian Hamiltonians, which can become defective at so-called exceptional points—points in parameter space which are typically associated with unconventional physics [8, 9]. The creation of popular non-Hermitian theories were soon followed by groundbreaking experimental successes in (mostly classical) optical systems demonstrating exceptional point physics [10–17].

Given the spectacular progress in $\mathcal{PT}$-symmetric optics, it is interesting to contemplate the consequences of non-Hermitian physics in essentially quantum optical systems [18–25]. Indeed, open quantum systems are a natural playground to study non-Hermitian effects due to their intrinsic description of system-environment interactions

* Author to whom any correspondence should be addressed.

Original Content from this work may be used under the terms of the Creative Commons Attribution 4.0 licence. Any further distribution of this work must maintain attribution to the author(s) and the title of the work, journal citation and DOI.

 © 2023 The Author(s). Published by IOP Publishing Ltd

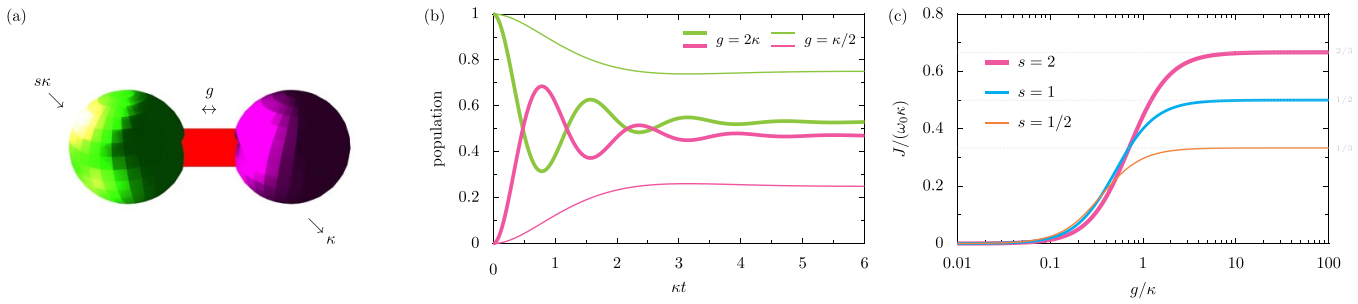

Figure 1. The unbalanced dimer and its populations. Panel (a): a pair of two-level systems, each of transition frequency ω_0, where the first qubit is pumped at a rate $s\kappa$, and the second qubit suffers loss at a rate κ. The coupling strength is g, and when the dimensionless parameter $s = 1$ the system is $\mathcal{PT}$-symmetric. Panel (b): the mean populations in the first (green) and second (pink) qubits as a function of time t (in units of κ^{-1}), for the cases of $g = 2\kappa$ (thick lines) and $g = \kappa/2$ (thin lines), with $s = 1$ (cf equation (8)). Panel (c): the steady state current J as a function of the coupling strength g (in units of $\omega_0\kappa$), for the cases of pumping associated with $s = \{1/2, 1, 2\}$ (cf equation (10)).

accounting for gain and loss [26, 27]. Perhaps the simplest case to consider is that of two coupled qubits [26–29], as described by the Hamiltonian $\hat{H}$ (we take $\hbar = 1$)

$$\hat{H} = \omega_0 \left(\sigma_1^\dagger \sigma_1 + \sigma_2^\dagger \sigma_2\right) + g\left(\sigma_1^\dagger \sigma_2 + \sigma_2^\dagger \sigma_1\right), \tag{1}$$

where ω_0 is the common transition frequency of both two-level systems (2LSs), and the coupling strength between them is accounted with $g \geqslant 0$. The raising and lowering operators $\sigma_n^\dagger$ and σ_n satisfy both the anticommutator relation $\{\sigma_n, \sigma_n^\dagger\} = 1$ and the rule $\sigma_1\sigma_2 = \sigma_2\sigma_1$, corresponding to two distinguishable qubits [30, 31]. Accounting for losses in an open quantum systems approach, we may employ the following quantum master equation for the system's density matrix ρ [29, 32]

$$\begin{aligned}\partial_t \rho = {} & \mathrm{i}[\rho, \hat{H}] \\ & + \frac{s\kappa}{2}\left(2\sigma_1^\dagger \rho \sigma_1 - \sigma_1\sigma_1^\dagger \rho - \rho\sigma_1\sigma_1^\dagger\right) \\ & + \frac{\kappa}{2}\left(2\sigma_2 \rho \sigma_2^\dagger - \sigma_2^\dagger\sigma_2\rho - \rho\sigma_2^\dagger\sigma_2\right),\end{aligned} \tag{2}$$

where the rate $\kappa \geqslant 0$ measures the loss out of the second 2LS, and the dimensionless parameter $s \geqslant 0$ tunes the overall gain rate $s\kappa$ into the first 2LS. Hence the gain-loss ratio amongst the coupled qubits is generally unbalanced (that is, as long as $s \neq 1$) as is sketched schematically in figure 1(a).

The time evolution of the density matrix ρ in equation (2) is governed by three ingredients. On the right-hand side of equation (2), the first line contains the Liouville–von Neumann commutator, involving the Hermitian Hamiltonian operator $\hat{H}$ of equation (1). The second line in equation (2) alludes to incoherent gain into the first qubit, and the third line in equation (2) contains the Lindbladian dissipator of the second qubit—these two additions impart non-Hermiticity into the model. Notably, we do not remove the so-called refilling (or feeding) terms from the two Lindbladians featuring in equation (2), and so we do not entertain the celebrated case of a traditional non-Hermitian Hamiltonian model [29]. Nevertheless, the quantum physics of non-Hermitian Hamiltonians is rather interesting, including for the promotion of squeezing and for the enhancement of quantum entanglement [33, 34].

We also note that the quantum optical master equation formalism that we employ in equation (2) is essentially equivalent to a more technically demanding quantum Langevin equation-style approach, since both approaches are unifiable within a higher-level quantum noise theory [35].

This considered minimal model of two coupled qubits, as encapsulated by equations (1) and (2), showcases a variety of quantum points of interest—including both exceptional points and critical points. These special points arise when the system parameters approach the values

$$s = 1, \qquad \mathcal{PT}\text{ symmetry}, \tag{3a}$$

$$g = \sqrt{s}\left(\frac{\sqrt{2} \pm 1}{2}\right)\kappa, \qquad \text{type} - \text{I MEP}, \tag{3b}$$

$$g = \frac{|s-1|}{4}\kappa, \qquad \text{type} - \text{II MEP}, \tag{3c}$$

$$g = \left(\frac{s+1}{2}\right)\kappa, \qquad \text{SCP}. \tag{3d}$$

Let us consider each quantum point of interest in the list of equation (3) in turn:

(*A*). In essentially classical systems, the border case between a system being open and being closed has received considerable attention. It was shown by Bender and co-workers [36, 37] that when $\mathcal{PT}$-symmetry is obeyed by an effective Hamiltonian, the resulting eigenvalues can be real despite the Hamiltonian being non-Hermitian. The prototypical $\mathcal{PT}$-symmetric system is that of two coupled harmonic oscillators [7], one being supplied with gain κ, and the other suffering loss at the equivalent rate κ. Then it follows that upon carrying out the parity operation (switching the positions of the two oscillators) and the time operation (flipping time, so that gain and loss are interchanged) the transformed system is equivalent to the starting one: thus $\mathcal{PT}$-symmetry is obeyed [7]. It was recently proposed by Huber and co-workers [26] that the natural operation extending $\mathcal{PT}$-symmetry to open quantum systems is to interchange loss and gain using the operator transformations $\sigma_1 \to \sigma_1^\dagger$ and $\sigma_2 \to \sigma_2^\dagger$ within the Lindblad

dissipators. Hence, for the setup we consider in figure 1(a), the system exhibits $\mathcal{PT}$ symmetry when the dimensionless parameter $s=1$, such that the gain and loss is indeed evenly balanced (cf equation (3*a*) and figure 1(a)).

(*B*). An intuitive way to write down an effective Hamiltonian $\mathcal{H}$ arising from a quantum master equation is to form the matrix equation for the mean values of the first moments, that is objects like $\langle\sigma_1\rangle$ and $\langle\sigma_2\rangle$. In the case of the considered equation (2), the resultant effective dynamical equation is [29]

$$\mathrm{i}\partial_t\psi = \mathcal{H}\psi, \tag{4}$$

where the effective Hamiltonian $\mathcal{H}$ is a 4×4 matrix

$$\mathcal{H} = \begin{pmatrix} \omega_0 - \mathrm{i}\frac{s\kappa}{2} & g & -2g & 0 \\ g & \omega_0 - \mathrm{i}\frac{\kappa}{2} & 0 & -2g \\ 0 & \mathrm{i}s\kappa & \omega_0 - \mathrm{i}\kappa\left(s+\frac{1}{2}\right) & -g \\ 0 & 0 & -g & \omega_0 - \mathrm{i}\kappa\left(1+\frac{s}{2}\right) \end{pmatrix}, \tag{5}$$

and where $\psi = (\langle\sigma_1\rangle, \langle\sigma_2\rangle, \langle\sigma_1^\dagger\sigma_1\sigma_2\rangle, \langle\sigma_1\sigma_2^\dagger\sigma_2\rangle)^{\mathrm{T}}$ collects the averaged first moment operators. The four complex eigenvalues of $\mathcal{H}$ (and their associated eigenvectors) coalesce at two distinct points, exactly when the conditions of equation (3*b*) are met — they are truly exceptional points or EPs. We call these EPs arising from the first moments of the system type − I MEPs. Strikingly, these EPs exist both in the $\mathcal{PT}$-symmetric arrangement ($s=1$) and outside this balanced setup ($s\neq 1$).

(*C*). Naturally, another appealing route to uncover EPs within an open quantum systems approach is to consider higher orders of the moments. For example, by considering the second moments of the system, objects like $\langle\sigma_1^\dagger\sigma_1\rangle$ and $\langle\sigma_2^\dagger\sigma_2\rangle$, the dynamical equation formed from the quantum master equation of equation (2) is given by

$$\mathrm{i}\,\partial_t\Psi = \mathcal{M}\Psi + \mathcal{P}, \tag{6}$$

where $\Psi = (\langle\sigma_1^\dagger\sigma_1\rangle, \langle\sigma_2^\dagger\sigma_2\rangle, \langle\sigma_1^\dagger\sigma_2\rangle, \langle\sigma_2^\dagger\sigma_1\rangle)^{\mathrm{T}}$ gathers the four second moments, and with the column vector driving term $\mathcal{P} = (\mathrm{i}s\kappa, 0, 0, 0)^{\mathrm{T}}$. Explicitly, the dynamical matrix $\mathcal{M}$ is defined via

$$\mathcal{M} = \begin{pmatrix} -\mathrm{i}s\kappa & 0 & g & -g \\ 0 & -\mathrm{i}\kappa & -g & g \\ g & -g & -\mathrm{i}\left(\frac{1+s}{2}\right)\kappa & 0 \\ -g & g & 0 & -\mathrm{i}\left(\frac{1+s}{2}\right)\kappa \end{pmatrix}, \tag{7}$$

which admits complex eigenvalues (and eigenvectors) which simultaneously coalesce at only one point (cf equation (3*c*)). This EP may be termed a type − II MEP due to its association with the second moments. Notably, here the EP vanishes when $s=1$, such that there is no type − II MEP when the system is in its $\mathcal{PT}$-symmetric, balanced arrangement.

(*D*). The quantum nature of the model of equation (2) naturally leads one to consider the explicitly quantum features which may be governed by truly quantum points of interest. Considerations of the properties of the density matrix ρ — and especially entanglement measures — lead to the observation of a critical (and non-exceptional) point. In particular, the critical point at which the quantum state suddenly becomes unentangled (or separable), which we dub a separable critical point (SCP), is given by equation (3*d*) in the steady state.

Let us mention that if we were to neglect the refilling terms in the Lindbladians appearing in equation (2) in order to enter a non-Hermitian Hamiltonian model regime, the two influential dynamical matrices discussed previously, $\mathcal{H}$ and $\mathcal{M}$ as defined in equations (5) and (7)] respectively, would be markedly different [29]. As a knock-on effect, the locations of the EPs (as well as the overall dynamics) also change significantly. However, there is the pronounced cost of the approximation employed (neglecting the refilling terms) highly restricting the parameters one may reasonably consider, such that we relegate a discussion of the non-Hermitian Hamiltonian aspects of the model to the supplementary material [29].

In what follows, we consider the impact of the four quantum points of interest listed in equation (3) in a handful of common observables and measures. In doing so, we highlight the importance of such analyses for complete descriptions of quantum optical systems with substantial non-Hermitian aspects (as they arise from a proper quantum master equation approach).

2. Populations

The mean values of the second moments $\langle\sigma_n^\dagger\sigma_n\rangle$ gives access to the average populations of the two qubits. The analytic expressions for the dynamic populations, with the initial conditions $\langle\sigma_1^\dagger\sigma_1\rangle = 1$ and $\langle\sigma_2^\dagger\sigma_2\rangle = 0$ at the starting time $t=0$, are particularly simple when the loss and gain are balanced (that is, when $s=1$). These two qubit populations, accessed from the solution of the equation of motion given in equation (6), then read [29, 38]

$$\langle\sigma_1^\dagger\sigma_1\rangle = \frac{\kappa^2+2g^2}{\kappa^2+4g^2} + \frac{2g^2\cos(2gt)+\kappa g\sin(2gt)}{\kappa^2+4g^2}\mathrm{e}^{-\kappa t}, \tag{8a}$$

$$\langle\sigma_2^\dagger\sigma_2\rangle = \frac{2g^2}{\kappa^2+4g^2} - \frac{2g^2\cos(2gt)+\kappa g\sin(2gt)}{\kappa^2+4g^2}\mathrm{e}^{-\kappa t}, \tag{8b}$$

which display exponential decay, with the time constant $1/\kappa$, of the trigonometric population oscillations towards unequal steady states (given by the first terms on the right-hand sides of equation (8)). Such behaviour for the left (green) and right (pink) qubits is displayed graphically in figure 1(b). When the coupling g is strong (thick lines) distinctive Rabi cycles of the populations may be observed. Otherwise, for weak coupling g (thin lines) there is a monotonic approach to the steady state population, which is created due to an equilibrium being found between the competing loss and gain processes.

The results for unbalanced arrangements of the qubits (where the dimensionless parameter $s\neq 1$) do indeed admit type − II MEPs (cf equation (3*c*)). However, the reconstruction of the population expressions of equation (8)

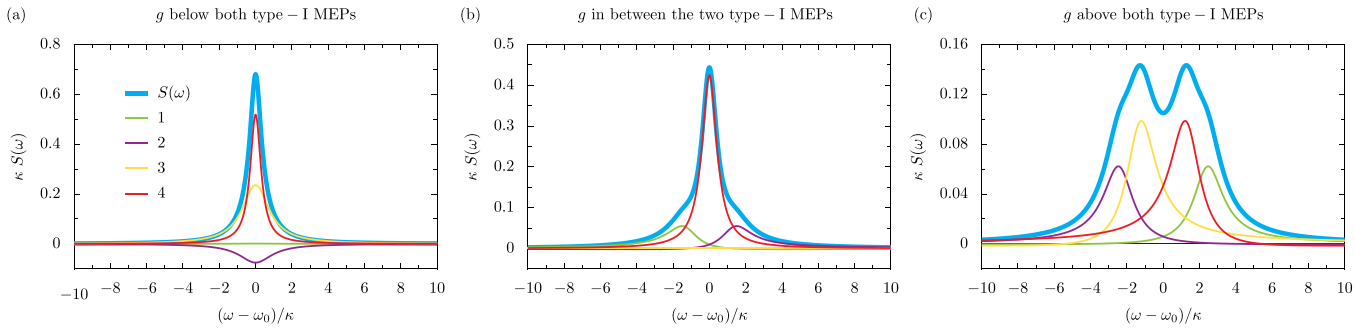

Figure 2. The optical spectrum $S(\omega)$, as a function of the shifted emission frequency $\omega-\omega_0$ (in units of κ), for the balanced case of $s=1$ (thick cyan lines). Panel (a): the coupling strength $g=\kappa/5$, which is below the first type − I MEP. Panel (b): $g=\kappa$, which is between the first and second type − I MEPs. Panel (c): $g=2\kappa$, which is above the second and final type − I MEP. Thin colored lines: the four contributions to the overall spectrum, due to the four possible transitions in the system (cf equation (12)). The type − I MEPs occur at $g=(\sqrt{2}-1)\kappa/2\simeq 0.207\kappa$ and $g=(\sqrt{2}+1)\kappa/2\simeq 1.207\kappa$ respectively (cf equation (3*b*)).

around these exceptional points (from damped-trigonometric to damped-algebraic) is not readily noticeable and so these results are not displayed here—although we do note that some signatures of these EPs have recently been obtained in reference [27].

The general analytic expressions for the steady state populations $\lim_{t\to\infty}\langle\sigma_n^\dagger\sigma_n\rangle$ are readily obtainable for any gain-loss imbalance, as judged by the dimensionless parameter s. The following neat formula for the population imbalance across the dimer system may then be found [29]

$$\lim_{t\to\infty}\frac{\langle\sigma_1^\dagger\sigma_1\rangle-\langle\sigma_2^\dagger\sigma_2\rangle}{\langle\sigma_1^\dagger\sigma_1\rangle+\langle\sigma_2^\dagger\sigma_2\rangle}=\frac{(s+1)\,\kappa^2}{8g^2+(s+1)\,\kappa^2}, \tag{9}$$

which is bounded between 0 and 1 for strong and weak couplings g respectively. The population imbalance of equation (9) suggests the formation of a steady state current across the duo of qubits is possible [39]. Indeed, the driving $s\kappa$ into the first 2LS and the loss κ out of the second 2LS allow for a nonzero steady state current J to be set up, with the strength [29]

$$J=\left(\frac{s}{s+1}\right)\frac{4g^2\kappa}{4g^2+s\kappa^2}\,\omega_0. \tag{10}$$

The current J displays the bounds $0\leqslant J\leqslant\omega_0\kappa s/(s+1)$ for weak and strong couplings g, as shown in figure 1(c) for several values of s. This current J could act as a useful observable to calibrate the coupled quantum system under experimental consideration.

3. Spectra

The quantum regression formula provides a route to the first-order correlation function $g_n^{(1)}(\tau)$ of the nth qubit. With the delay time $\tau\geqslant 0$, this degree of coherence may be defined, using the steady state population as normalization, as $g_n^{(1)}(\tau)=\lim_{t\to\infty}\langle\sigma_n^\dagger(t)\sigma_n(t+\tau)\rangle/\langle\sigma_n^\dagger(t)\sigma_n(t)\rangle$. By definition, $|g_n^{(1)}(0)|=1$ demonstrates full coherence, $|g_n^{(1)}(0)|=0$ perfect incoherence and otherwise $0<|g_n^{(1)}(0)|<1$ partial coherence [32]. Analytical formulas for $g_n^{(1)}(\tau)$ are rather long in general, but simplify in the balanced case of $s=1$ to [29]

$$g_1^{(1)}(\tau)=\frac{\mathrm{e}^{-\mathrm{i}\omega_0\tau}\mathrm{e}^{-\kappa\tau}}{\kappa^2+2g^2}\left\{\frac{\kappa^2+\kappa g+2g^2}{2}\cos(q\tau)+\frac{\kappa^2-\kappa g+2g^2}{2}\cos(p\tau)+\frac{\kappa^2(3g+\kappa)}{4q}\sin(q\tau)-\frac{\kappa^2(3g-\kappa)}{4p}\sin(p\tau)\right\}, \tag{11a}$$

$$g_2^{(1)}(\tau)=\frac{\mathrm{e}^{-\mathrm{i}\omega_0\tau}\mathrm{e}^{-\kappa\tau}}{4g}\left\{(2g+\kappa)\cos(q\tau)+(2g-\kappa)\cos(p\tau)+\frac{\kappa(4g+\kappa)}{2q}\sin(q\tau)+\frac{\kappa(4g-\kappa)}{2p}\sin(p\tau)\right\}, \tag{11b}$$

where we have introduced the auxiliary functions $q=\sqrt{g^2-g\kappa-\kappa^2/4}$ and $p=\sqrt{g^2+g\kappa-\kappa^2/4}$. Total incoherence arises at long times, $g_n^{(1)}(\infty)=0$, due to the lack of correlations with large time delays τ.

The optical spectrum $S(\omega)$ of the first (and driven) qubit may be calculated directly from the degree of coherence $g_1^{(1)}(\tau)$, via the normalized spectral formula $S(\omega)=\lim_{t\to\infty}\mathrm{Re}\int_0^\infty g_1^{(1)}(\tau)/\pi$ [40, 41]. There are four possible transitions in the coupled system (in the simplest case of the bare states, they are from $|1,1\rangle\to|1,0\rangle\,\&\,|0,1\rangle$ and from $|1,0\rangle\,\&\,|0,1\rangle\to|0,0\rangle$) which are all associated with a certain transition frequency and a certain lifetime. Therefore, there are four contributions (thin colored lines) to the overall spectrum $S(\omega)$ (thick cyan lines) with particular peak positions and broadenings, as is shown in figures 2(a)–(c). The positions and broadenings may be determined via the real and imaginary parts respectively of the four complex eigenvalues $\epsilon_{\pm,\pm}$, arising from the governing dynamical matrix $\mathcal{H}$ of equation (5), which read [29]

$$\epsilon_{\pm,\pm}=\omega_0-\mathrm{i}\kappa\pm\sqrt{g^2-\left(\frac{\kappa}{2}\right)^2}\pm g\kappa. \tag{12}$$

This expression contains two points of coalescence, consistent with the type − I MEPs of equation (3*b*). Across the row

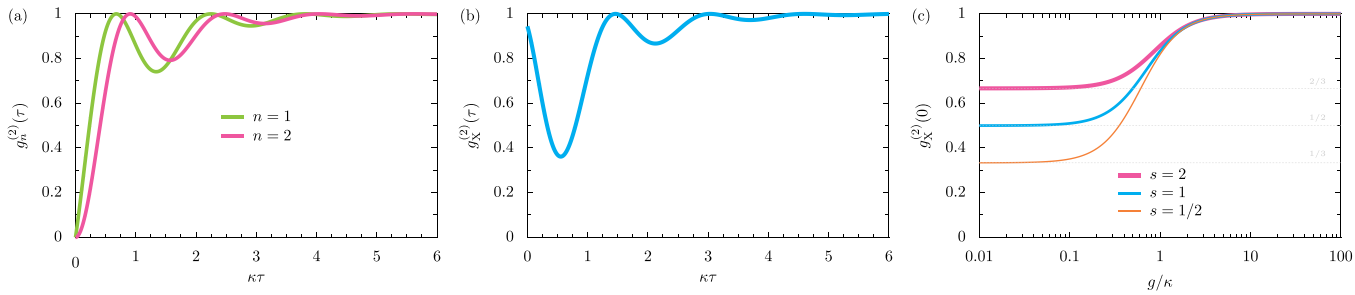

Figure 3. The unbalanced dimer and its correlations. Panel (a): second-order direct correlation function $g_n^{(2)}(\tau)$ as a function of the delay time τ (in units of κ^{-1}) for the first ($n=1$) and second ($n=2$) resonators (cf equations (13*a*) and (13*b*)), with $s=1$. Panel (b): second-order cross-correlation function $g_X^{(2)}(\tau)$, as a function of the delay time τ, with $s=1$ (cf equation (13*c*)). Panel (c): second-order cross-correlation function at zero delay $g_X^{(2)}(0)$, as a function of the coupling strength g (in units of κ), for the cases of $s=\{1/2,1,2\}$ (cf equation (14)).

of panels in the spectral figure 2, we consider three successively increasing values of the coupling strength g for the balanced case of $s=1$, so that the type$-$I MEPs occur at $g=(\sqrt{2}-1)\kappa/2\simeq 0.207\kappa$ and $g=(\sqrt{2}+1)\kappa/2\simeq 1.207\kappa$ (cf equation (3*b*)). In panel (a) the coupling strength g is below the first type$-$I MEP, and the spectrum $S(\omega)$ presents a singlet structure since the complex eigenvalues describing the transitions all have ω_0 as the real part and four distinct imaginary parts leading to four different spectral broadenings (cf equation (12)). Between the first type$-$I MEP and the second type$-$I MEP, there are three distinct real parts of the complex eigenvalues (since the first type$-$I MEP has been passed, associated with a coalescence) such that the singlet has developed noticeable spectral shoulders in panel (b). Finally in panel (c), above the second and final type$-$I MEP, the four distinct real parts of the complex eigenvalues (cf equation (12)) lead to a characteristic doublet spectrum with significant spectral shoulders. Hence the evolution with g of the number of peaks within the optical spectrum $S(\omega)$ presents a useful and rather vivid indicator for when the system has passed through type$-$I MEPs.

4. Correlations

The degree of second-order coherences $g^{(2)}(\tau)$ measure the emission properties of the duo of coupled qubits [32]. The normalized second-order correlation functions are defined by, for the two direct correlation functions: $g_n^{(2)}(\tau)=\lim_{t\to\infty}\langle\sigma_n^\dagger(t)\sigma_n^\dagger(t+\tau)\sigma_n(t+\tau)\sigma_n(t)\rangle/\langle\sigma_n^\dagger(t)\sigma_n(t)\rangle^2$, with $n=\{1,2\}$. These correlators count the probabilities of two emissions, with a time delay τ, from the same qubit. Likewise, the cross-correlator is similarly given by $g_X^{(2)}(\tau)=\lim_{t\to\infty}\langle\sigma_1^\dagger(t)\sigma_2^\dagger(t+\tau)\sigma_2(t+\tau)\sigma_1(t)\rangle/(\langle\sigma_1^\dagger(t)\sigma_1(t)\rangle\langle\sigma_2^\dagger(t)\sigma_2(t)\rangle)$, which tracks two τ-delayed emissions, one from each qubit in the dimer.

The explicit expressions for these types of $g^{(2)}(\tau)$ are most simple in the balanced case of $s=1$, where they read [29]

$$g_1^{(2)}(\tau)=1-\frac{\left[\left(2g^2+\kappa^2\right)\cos\left(g\tau\right)-g\kappa\sin\left(g\tau\right)\right]^2}{\left(2g^2+\kappa^2\right)^2}\mathrm{e}^{-\kappa\tau}, \tag{13a}$$

$$g_2^{(2)}(\tau)=1-\frac{\left[2g\cos\left(g\tau\right)+\kappa\sin\left(g\tau\right)\right]^2}{4g^2}\mathrm{e}^{-\kappa\tau}, \tag{13b}$$

$$g_X^{(2)}(\tau)=1-\frac{\left[g\kappa\cos\left(g\tau\right)+\left(2g^2+\kappa^2\right)\sin\left(g\tau\right)\right]^2}{2g^2\left(2g^2+\kappa^2\right)}\mathrm{e}^{-\kappa\tau}. \tag{13c}$$

We plot the two direct correlation functions $g_n^{(2)}(\tau)$ in figure 3(a), where $n=1$ is marked with the green line and $n=2$ by the pink line. At zero time delay ($\tau=0$), the two-level nature of the qubits enforces $g_n^{(2)}(0)=0$, since a finite time τ is required for the qubit to be re-excited from the ground state in order to emit a second photon. For nonzero τ the phenomena of antibunching, as defined by $g_n^{(2)}(0)<g_n^{(2)}(\tau)$ emerges as a non-classical effect. The long time limit ($\tau\to\infty$) sees perfect coherence being approached due to the random nature of the emissions in this asymptotic scenario.

We plot the cross-correlation function $g_X^{(2)}(\tau)$, as defined in equation (13*c*), in figure 3(b). The result $g_X^{(2)}(0)\neq 0$ arises since simultaneous emissions, one in each qubit, are possible even at zero time delay ($\tau=0$). Thereafter, there are characteristic oscillations until the asymptotic result $g_X^{(2)}(\infty)=1$ is approached, signifying the qubits are behaving independently for large delay times τ. At zero delay ($\tau=0$), and for a general unbalanced system with any s, we find the cross-correlation formula

$$g_X^{(2)}(0)=\frac{4g^2+s\kappa^2}{4g^2+(s+1)\kappa^2}. \tag{14}$$

We plot $g_X^{(2)}(0)$ in figure 3(c) as a function of the coupling g for three values of s, showcasing the weak coupling limit of $g_X^{(2)}(0)=1/(1+s)$, and the strong coupling result of $g_X^{(2)}(0)=1$, such that the degree of antibunching can be somewhat tuned by the pumping strength $s\kappa$. Similar to the population dynamics, the correlation functions considered (with $s\neq 1$) do not allow for as striking a fingerprint of an exceptional point as compared to the optical spectrum, since the behaviour of the relevant functions at the exceptional point is rather similar to the behaviour immediately above and below it.

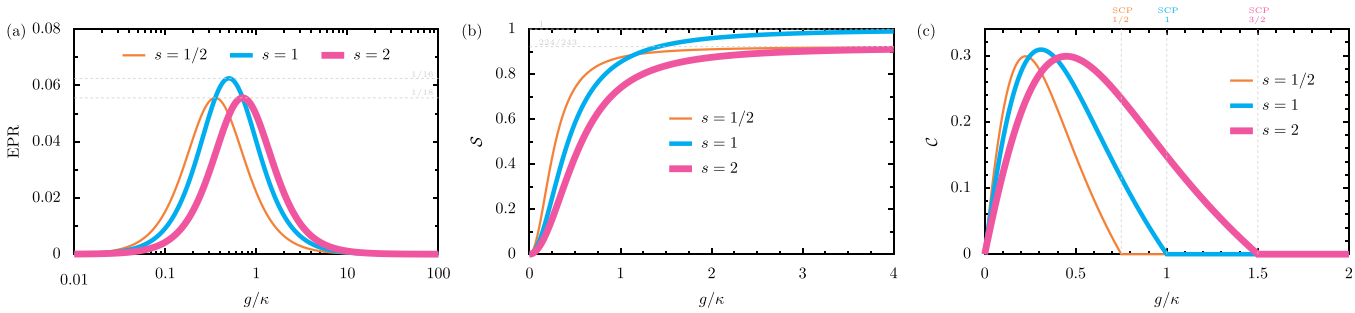

Figure 4. The unbalanced dimer and its quantum information in the steady state. Panel (a): the entanglement measure EPR as a function of the coupling strength g (in units of κ) for the cases of $s = \{1/2, 1, 2\}$ (cf equation (15)). Dashed grey lines: the maximum values of $1/16 \simeq 0.063$ and $1/18 \simeq 0.056$. Panel (b): the linear entropy $\mathcal{S}$ as a function of the scaled coupling strength g/κ (cf equation (16)). Dashed grey lines: the asymptotic values of 1 and $224/243 \simeq 0.92$. Panel (c): the concurrence $\mathcal{C}$ as a function of the scaled coupling strength g/κ. Dashed grey lines: the concurrence zeroes first occur at $1/2$, 1 and $3/2$, matching the SCPs of equation (3*d*).

5. Informatics

Let us now consider some measures typically used in quantum information science—such as purity, linear entropy, concurrence and negativity—and the impact upon them of the special points of interest listed in equation (3), be they exceptional or otherwise. In particular, we are interested in the response of the system in the steady state. Notably, the steady-state entanglement properties of two coupled qubits is known to be important for quantum information processing and device design [42–46].

The measure EPR frequently arises in quantum metrology, where the inequality $\mathrm{EPR} > 0$ suggests entanglement [47]. Considering the steady state with the asymptotic time $t \to \infty$, and coming directly from the definition of $\mathrm{EPR} = \lim_{t\to\infty}(\langle\sigma_1^\dagger\sigma_1\rangle\langle\sigma_2^\dagger\sigma_2\rangle - \langle\sigma_1^\dagger\sigma_1\sigma_2^\dagger\sigma_2\rangle)$, we obtain this key measure as [29]

$$\mathrm{EPR} = \left(\frac{s}{s+1}\frac{2g\kappa}{4g^2+s\kappa^2}\right)^2, \tag{15}$$

which exhibits the lower bound of 0 for both weak and strong coupling ($g \ll \kappa$ and $g \gg \kappa$ respectively), and the upper bound of $s/[2(1+s)]^2$ at the certain coupling strength $g = \sqrt{s}\kappa/2$. We plot the EPR in figure 4(a) as a function of g, showcasing the stronger EPR entanglement for moderate coupling values and how it vanishes for extremely weak or strong couplings, such that no exceptional or critical points influence this simple measure.

The linear entropy $\mathcal{S}$ is a common measure of the mixedness of a quantum state ρ. This quantity may be defined by $\mathcal{S} = (4/3)[1 - \mathrm{Tr}(\rho^2)]$, where the prefactor of $4/3$ ensures that the bounds fulfil $\mathcal{S} \in [0, 1]$. The lower bound corresponds to a pure state and the upper bound to a maximally mixed state. In the steady state, the linear entropy $\mathcal{S}$ for the unbalanced qubit system reads [29]

$$\mathcal{S} = \frac{32}{3}\frac{s}{(s+1)^4}\left(\frac{g}{4g^2+s\kappa^2}\right)^2 \times\left\{(1+s^2)(1+s)^2\kappa^2 + 8(s^2+s+1)g^2\right\}. \tag{16}$$

We plot the linear entropy in figure 4(b) as a function of the coupling g, which highlights the total purity of the state with small couplings $g \ll \kappa$ as may be expected. The monotonic rise in mixedness of the state with increasing coupling g eventually plateaus at a value given by $\mathcal{S} \simeq 16s(1+s+s^2)/[3(1+s)^4]$. Hence, only with balanced coupling ($s = 1$) does a maximally mixed state arise with $\mathcal{S} = 1$ identically.

The concurrence $\mathcal{C}$, as developed by Wooters [48, 49], is a celebrated entanglement measure of bipartite mixed states. Zero concurrence is associated with a separable state, while nonzero concurrence measures the degree of entanglement of the state (up to a maximum of unity for maximum entanglement). We consider the steady state concurrence $\mathcal{C}$ as a function of the coupling strength g in figure 4(c) for the cases of $s = \{1/2, 1, 2\}$. Strikingly, there are critical points at which the steady state concurrence suddenly drops to zero such that the state becomes separable—we calls these points separable critical points or SCPs (cf equation (3*d*)). Otherwise, in the region of nonzero entanglement one finds (for the balanced case of $s = 1$) the maximal obtainable concurrence

$$\max\{\mathcal{C}\} = \frac{1}{1+\sqrt{5}} \simeq 0.309\ldots, \tag{17}$$

which occurs with the moderate coupling $g = \kappa/(1+\sqrt{5}) \simeq 0.309\kappa$, and which is slightly higher than the maximum values of $\mathcal{C}$ for the unbalanced arrangements of the qubits. The entanglement-disentanglement transitions in figure 4(c) are wholly governed by equation (3*d*), which is a useful quantum point of interest in addition to the exceptional points of the system.

6. Thermodynamic limit

The results for the considered coupled qubits (cf equation (1)) may be approached from the analogous model of two coupled quantum harmonic oscillators by truncating the number of energy levels N of each oscillator. In the untruncated limit ($N \to \infty$), the pure coupled oscillator system admits the following quantum points of interest [29]

$$g = \left(\frac{s+1}{4}\right)\kappa, \qquad \begin{cases}\text{type} - \text{I MEP},\\ \text{type} - \text{II MEP},\end{cases} \tag{18a}$$

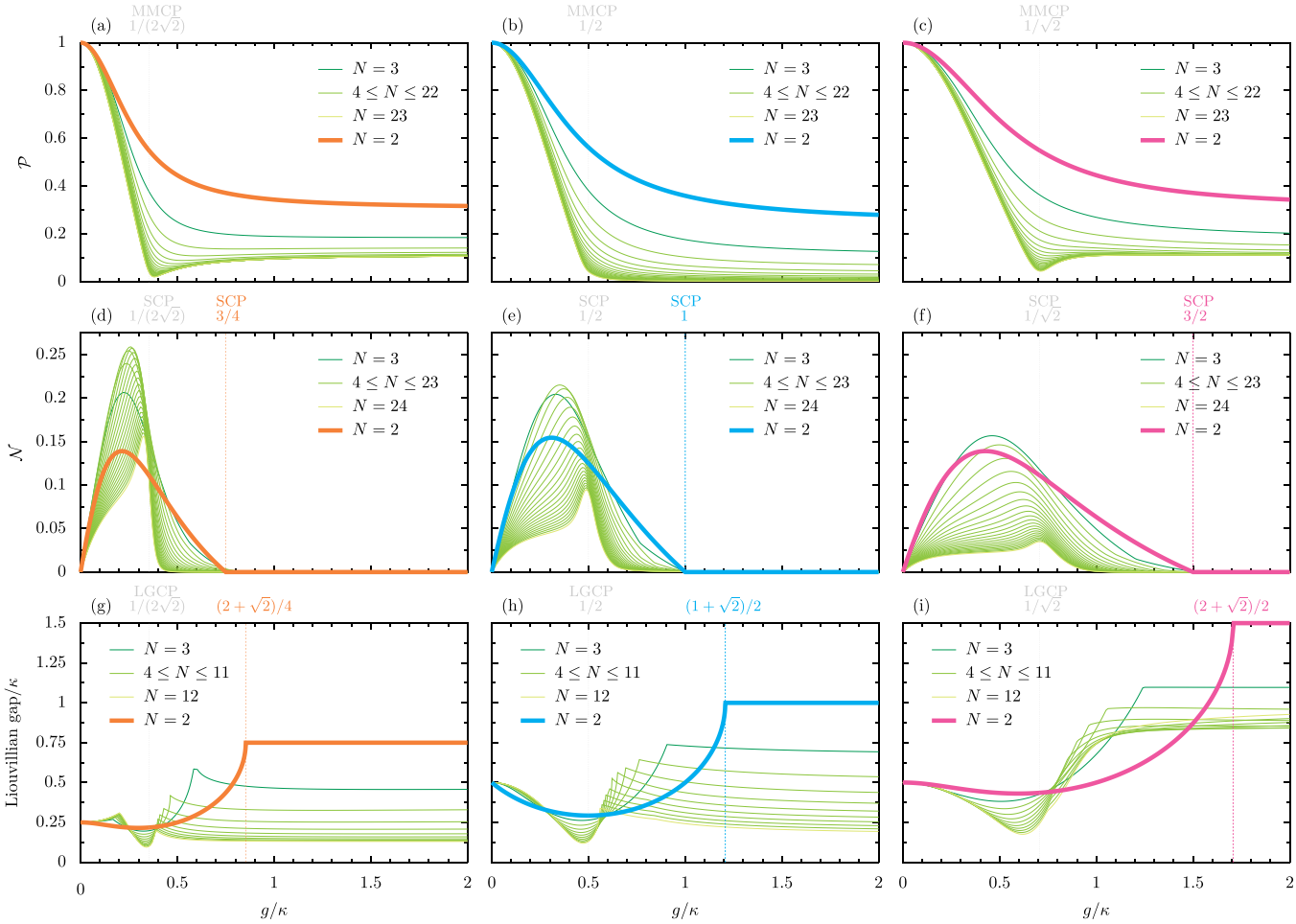

Figure 5. The unbalanced dimer beyond the two-level limit. We consider the steady state ($t \to \infty$) regime, and the two-level system results are denoted by thick orange, cyan and pink lines for the cases of $s = \{1/2, 1, 2\}$ respectively. Also shown are the results for a pair of truncated quantum harmonic oscillators: the number of levels of each oscillator is N, so that $N = 2$ recovers the two-level system results while untruncated oscillators are approached in the $N \gg 2$ limit (thin green lines). Panels (a)–(c): the purity $\mathcal{P}$ as a function of the coupling strength g (in units of κ). Dotted grey lines: the values of interest as $N \gg 2$ are $1/(2\sqrt{2}) \simeq 0.354$, $1/2$ and $1/\sqrt{2} \simeq 0.707$ for panels (a)–(c) respectively, aligning with the MMCP for the coupled oscillators (cf equation (18*b*)). Panels (d)–(f): as for the upper panels, but instead showing the negativity $\mathcal{N}$ as a function of g. Dotted grey lines: the values of interest as $N \gg 2$ are $1/(2\sqrt{2}) \simeq 0.354$, $1/2$ and $1/\sqrt{2} \simeq 0.707$ for panels (d)–(f) respectively, aligning with the SCP for the coupled oscillators (cf equation (18*b*)). Dashed grey lines: the negativity zeroes along the top row of panels occur at $3/4$, 1 and $3/2$ respectively for $N = 2$, which are the qubit SCPs (cf equation (3*d*)). Panels (g)–(i): as for the upper panels, but instead showing the Liouvillian gap as a function of g. Dotted grey lines: the values of interest as $N \gg 2$ are $1/(2\sqrt{2}) \simeq 0.354$, $1/2$ and $1/\sqrt{2} \simeq 0.707$ for panels (g)–(i) respectively, these points are Liouvillian gap critical points (LGCPs) for the coupled oscillators (cf equation (18*b*)). Dashed grey lines: the Liouvillian gap plateaus along the bottom row of panels occur at $(\sqrt{2}+2)/4 \simeq 0.85$, $(\sqrt{2}+1)/2 \simeq 1.21$ and $(\sqrt{2}+2)/\sqrt{2} \simeq 1.71$ respectively for $N = 2$, aligning with the largest type $-$ I MEP for the coupled qubits (cf equation (3*b*)).

$$g = \frac{\sqrt{s}}{2}\kappa, \qquad \begin{cases} \text{MMCP}, \\ \text{SCP}, \\ \text{LGCP}. \end{cases} \tag{18b}$$

Notably, the type $-$ I and type $-$ II MEPs coincide for this ($N \to \infty$ level) linear model (equation (18*a*)), in stark contrast to the qubit case with $N = 2$ levels (equations (3*a*) and (3*b*)). Interestingly, there is also a coexistence of the SCP and the LGCP, defined as the point in parameter space at which the Liouvillian gap closes, which can indeed occur in the thermodynamic limit of $N \to \infty$. Additionally, there is a further coincidence in equation (18*b*) with the maximally mixed critical point (MMCP), which is associated with purity of the state becoming zero.

In what follows, we consider a handful of illuminating quantum steady state properties in the extreme limits of $N = 2$ for coupled qubits, $N \to \infty$ for coupled quantum harmonic oscillators, and otherwise for some values of N in between these instructive limits.

Let us first consider the purity $\mathcal{P}$ of the system, a measure of the mixedness of the state ρ as defined by $\mathcal{P} = \text{Tr}(\rho^2)$, so that $\mathcal{P} = 1$ corresponds to a pure state and $\mathcal{P} = 1/D$ to a maximally mixed state (here D is the dimension of the Hilbert space in question). The top row of figure 5 displays the steady

state purity $\mathcal{P}$ as a function of the coupling strength g, for the cases of $s=\{1/2,1,2\}$ in panels (a)–(c) respectively. The qubit ($N=2$) results are given by the thick colored lines in the figure, and are described by the exact expression

$$\mathcal{P}=\frac{16g^2\left[s^2(1+s)^2\kappa^2+(1+s^2)^2g^2\right]+s^2(1+s)^4\kappa^4}{(1+s)^4\left(4g^2+s\kappa^2\right)^2}, \tag{19}$$

which is necessarily unity with vanishing coupling g. The truncated oscillator results are represented by the thin green lines in figures 5(a)–(c), and for greater visibility the edge cases of $N=3$ and $N=20$ are given by dark green and light green lines respectively. Notably, with increasing the number of levels N the purity $\mathcal{P}$ tends towards zero—suggesting maximal mixedness—at the MMCP defined by equation (18*b*), which is marked by the dotted grey lines in the figure.

The negativity $\mathcal{N}$ is a popular quantifier of how much entanglement is contained within a quantum state ρ [50, 51]. This quantity is zero for separable states and nonzero for entangled states. Defined as the absolute sum of the negative eigenvalues of the partial transpose of the state ρ, it may be computed exactly in the steady state and for the $N=2$ level case as [29]

$$\mathcal{N}=\frac{2g}{4g^2+s\kappa^2}\left\{\sqrt{(s-1)^2g^2+s^2\kappa^2}-\left(\frac{s^2+1}{s+1}\right)g\right\} \times\frac{1}{s+1}\Theta\left(\tfrac{s+1}{2}\kappa-g\right), \tag{20}$$

where $\Theta(x)$ is the Heaviside theta function. The presence of the step function within equation (20) highlights the hard border between entangled and unentangled states at the critical points defined by equation (3*d*) for the qubit ($N=2$) case. For example, within the balanced arrangement of the qubit dimer ($s=1$) we find the maximal negativity $\max\{\mathcal{N}\}=1/(2+2\sqrt{5})\simeq 0.155$ occurs at $g=\kappa/(1+\sqrt{5})\simeq 0.309$, while the SCP may be found at $g=\kappa/2$. This circumstance is plotted as the thick cyan line in figure 5(e), while the panels (d) and (f) show the equivalent results for the unbalanced cases of $s=1/2$ (thick orange line) and $s=2$ (thick pink line) respectively, where the qubit SCPs are denoted by the dashed colored lines. The cases of truncated oscillators are shown in the second row of figure 5 by thin green lines. Notably, in the thermodynamic limit $N\to\infty$ the coupled oscillator negativities $\mathcal{N}$ in figures 5(d)–(f) seemingly go to zero at the SCPs predicted by equation (18*b*), which are marked by the dotted grey lines in the figure. This statement is most easily seen in panel (d), and more supporting evidence for this claim is presented in [29].

The Liouvillian spectral gap is defined from the complex eigenvalue of the Liouvillian with the smallest real part (after removing any zero eigenvalues from consideration) [52–54]. The closing of the Liouvillian gap, which is possible in the thermodynamic limit $N\to\infty$, may occur at a critical value of some system parameter. This gap closing phenomena is associated with a dissipative phase transition, which have already been measured in a handful of modern photonic architectures [55–57]. We plot the Liouvillian gap as a function of the coupling strength g in figures 5(g)–(i) for three different values of s. The coupled qubit ($N=2$) results are denoted by thick colored lines and cannot lead to a closing of the Liouvillian gap due to the finite size of the Hilbert space, however the plateau feature arises due to the largest type − I MEP (cf equation (3*b*)). Interestingly, the truncated oscillator results (thin green lines) suggest a closing of the gap in the large N limit exactly at the LGCP of equation (18*b*). This trend of gap closing is best seen in panel (g), and more supporting evidence for this claim is given in [29].

Overall, by truncating the linear harmonic oscillator model to recover the qubits results, one notices the evolution of the SCPs in the middle row of figure 5, describing the movement in g/κ-space of the entanglement-disentanglement transitions in the steady state. The consideration of a thermodynamic limit with the coupled oscillators also revealed the critical points that we have dubbed MMCP and LGCP, governing the mixedness zero and the dissipative phase transition in the system using equation (18*b*), which complement the more celebrated exceptional points of the oscillator model (cf equation (18*a*)).

7. Discussion

In conclusion, we have considered a simple quantum optical model of two coupled qubits experiencing both loss and gain. In analogy to the (essentially semiclassical) exceptional points found when using non-Hermitian Hamiltonians to model optical systems, here we have elucidated the many flavours of quantum points of interest — both exceptional and critical — which should appear in quantum optical systems describable within an open quantum systems approach. In particular, we have suggested that a change in the number of peaks in the optical spectrum can be a neat signifier of movement through a certain flavour of first moment exceptional point, while steady state entanglement measures abruptly becoming zero are associated with passing past a certain critical point. Following a series of recent pioneering experiments in quantum non-Hermitian physics — primarily exploiting superconducting qubits [58–70] — we hope that our theoretical results can stimulate further experimental work in the study of quantum points of interest, broadly interpreted, and their distinctive physical consequences.

Data availability statements

All data that support the findings of this study are included within the article (and any supplementary files).

Acknowledgments

Funding: C A D is supported by the Royal Society via a University Research Fellowship (URF/ R1/ 201158). O I R F is funded by the EPSRC via the Maths DTP 2021-22 University of Exeter (EP/W523859/1). *Discussions*: We thank V A Saroka for fruitful discussions.

ORCID iD

Charles Andrew Downing https://orcid.org/0000-0002-0058-9746

References

[1] Bender C M 2007 Making sense of non-Hermitian Hamiltonians *Rep. Prog. Phys.* **70** 947
[2] Moiseyev N 2011 *Non-Hermitian Quantum Mechanics* (Cambridge University Press)
[3] Ashida Y, Gong Z and Ueda M 2020 Non-Hermitian physics *Adv. Phys.* **69** 249–435
[4] Konotop V V, Yang J and Zezyulin D A 2016 Nonlinear waves in $\mathcal{PT}$-symmetric systems *Rev. Mod. Phys.* **88** 035002
[5] El-Ganainy R, Makris K G, Khajavikhan M, Musslimani Z H, Rotter S and Christodoulides D N 2018 Non-Hermitian physics and $\mathcal{PT}$ symmetry *Nat. Phys.* **14** 11
[6] Miri M-A and Alu A 2019 Exceptional points in optics and photonics *Science* **363** 6422
[7] Ozdemir S K, Rotter S, Nori F and Yang L 2019 Parity-time symmetry and exceptional points in photonics *Nat. Mater.* **18** 783
[8] Berry M V 2004 Physics of nonhermitian degeneracies *Czech. J. Phys.* **54** 1039
[9] Heiss W D 2004 Exceptional points—their universal occurrence and their physical significance *Czech. J. Phys.* **54** 1091
[10] Ruter C E, Makris K G, El-Ganainy R, Christodoulides D N, Segev M and Kip D 2010 Observation of parity-time symmetry in optics *Nat. Phys.* **6** 192
[11] Feng L, Wong Z J, Ma R-M, Wang Y and Zhang X 2014 Single-mode laser by parity-time symmetry breaking *Science* **346** 972
[12] Hodaei H, Miri M-A, Heinrich M, Christodoulides D N and Khajavikhan M 2014 Parity-time-symmetric microring lasers *Science* **346** 975
[13] Hodaei H, Hassan A U, Wittek S, Garcia-Gracia H, El-Ganainy R, Christodoulides D N and Khajavikhan M 2017 Enhanced sensitivity at higher-order exceptional points *Nature* **548** 187
[14] Wu Y, Liu W, Geng J, Song X, Ye X, Duan C-K, Rong X and Du J 2019 Observation of parity-time symmetry breaking in a single-spin system *Science* **364** 878
[15] Xia S, Kaltsas D, Song D, Komis I, Xu J, Szameit A, Buljan H, Makris K G and Chen Z 2021 Nonlinear tuning of $\mathcal{PT}$ symmetry and non-Hermitian topological states *Science* **372** 72
[16] Wang C, Sweeney W R, Stone A D and Yang L 2021 Coherent perfect absorption at an exceptional point *Science* **373** 1261
[17] Ergoktas M S *et al* 2022 Topological engineering of terahertz light using electrically tunable exceptional point singularities *Science* **376** 184
[18] Prosen T 2012 $\mathcal{PT}$-Symmetric quantum Liouvillean dynamics *Phys. Rev. Lett.* **109** 090404
[19] Prosen T 2012 Generic examples of $\mathcal{PT}$-symmetric qubit (spin-1/2) Liouvillian dynamics *Phys. Rev.* A **86** 044103
[20] Am-Shallem M, Kosloff R and Moiseyev N 2012 Exceptional points for parameter estimation in open quantum systems: analysis of the Bloch equations *New J. Phys.* **17** 113036
[21] Kepesidis K V, Milburn T J, Huber J, Makris K G, Rotter S and Rabl P 2016 $\mathcal{PT}$-symmetry breaking in the steady state of microscopic gain–loss systems *New J. Phys.* **18** 095003
[22] Minganti F, Miranowicz A, Chhajlany R W and Nori F 2019 Quantum exceptional points of non-Hermitian Hamiltonians and Liouvillians: the effects of quantum jumps *Phys. Rev.* A **100** 062131
[23] Jaramillo Avila B, Ventura-Velazquez C, Leon-Montiel R de J, Joglekar Y N and Rodriguez-Lara B M 2020 $\mathcal{PT}$-symmetry from Lindblad dynamics in a linearized optomechanical system *Sci. Rep.* **10** 1761
[24] Arkhipov I I, Miranowicz A, Minganti F and Nori F 2020 Quantum and semiclassical exceptional points of a linear system of coupled cavities with losses and gain within the Scully-Lamb laser theory *Phys. Rev.* A **101** 013812
[25] Downing C A and Saroka V A 2021 Exceptional points in oligomer chains *Commun. Phys.* **4** 254
[26] Huber J, Kirton P, Rotter S and Rabl P 2020 Emergence of $\mathcal{PT}$-symmetry breaking in open quantum systems *SciPost Phys.* **9** 052
[27] Khandelwal S, Brunner N and Haack G 2021 Signatures of Liouvillian exceptional points in a quantum thermal machine *PRX Quantum* **2** 040346
[28] Downing C A, López Carre no J C, Fernández-Domínguez A I and del Valle E 2020 Asymmetric coupling between two quantum emitters *Phys. Rev.* A **102** 013723
[29] Please see the supplementary material for the background theory supporting the results reported in the main text. It includes a discussion of the refilling terms in the quantum master equation of equation (2), and the physics of the non-Hermitian Hamiltonian limit of the coupled qubit model
[30] Allen L and Eberly J H 1975 *Optical Resonance and Two-Level Atoms* (Wiley)
[31] Downing C A and Zueco D 2021 Non-reciprocal population dynamics in a quantum trimer *Proc. R. Soc.* A **477** 20210507
[32] Gardiner C and Zoller P 2014 *The Quantum World of Ultra-Cold Atoms and Light, Book I: Foundations of Quantum Optics* (Imperial College Press)
[33] Lee T E, Reiter F and Moiseyev N 2014 Entanglement and spin squeezing in non-Hermitian phase transitions *Phys. Rev. Lett.* **113** 250401
[34] Ramirez R and Reboiro M 2019 Optimal spin squeezed steady state induced by the dynamics of non-Hermitian Hamiltonians *Phys. Scr.* **94** 085220
[35] Gardiner C W 1988 Quantum noise and quantum Langevin equations *IBM J. Res. Develop.* **32** 127
[36] Bender C M and Boettcher S 1998 Real spectra in non-Hermitian Hamiltonians having $\mathcal{PT}$ symmetry *Phys. Rev. Lett.* **80** 5243
[37] Bender C M 2018 *$\mathcal{PT}$ Symmetry: in Quantum and Classical Physics* (World Scientific)
[38] Downing C A and Sturges T J 2022 Directionality between driven-dissipative resonators *Europhys. Lett.* **140** 35001
[39] Manzano D, Tiersch M, Asadian A and Briegel H J 2012 Quantum transport efficiency and Fourier's law *Phys. Rev.* E **86** 061118
[40] del Valle E 2010 Strong and weak coupling of two coupled qubits *Phys. Rev.* A **81** 053811
[41] Downing C A, del Valle E and Fernández-Domínguez A I 2023 Resonance fluorescence of two asymmetrically pumped and coupled two-level systems *Phys. Rev.* A **107** 023717
[42] Plenio M B and Huelga S F 2002 Entangled light from white noise *Phys. Rev. Lett.* **88** 197901
[43] Hartmann L, Dur W and Briegel H-J 2006 Steady-state entanglement in open and noisy quantum systems *Phys. Rev.* A **74** 052304
[44] del Valle E 2011 Steady-state entanglement of two coupled qubits *J. Opt. Soc. Am.* B **28** 228
[45] Gonzalez-Tudela A, Martin-Cano D, Moreno E, Martin-Moreno L, Tejedor C and Garcia-Vidal F J 2011 Entanglement of two qubits mediated by one-dimensional plasmonic waveguides *Phys. Rev. Lett.* **106** 020501

[46] Decordi G L and Vidiella-Barranco A 2020 Sudden death of entanglement induced by a minimal thermal environment *Opt. Commun.* **475** 126233
[47] Pudlik T, Hennig H, Witthaut D and Campbell D K 2013 Dynamics of entanglement in a dissipative Bose-Hubbard dimer *Phys. Rev.* A **88** 063606
[48] Hill S A and Wootters W K 1997 Entanglement of a pair of quantum bits *Phys. Rev. Lett.* **78** 5022
[49] Wootters W K 1998 Entanglement of formation of an arbitrary state of two qubits *Phys. Rev. Lett.* **80** 2245
[50] Zyczkowski K, Horodecki P, Sanpera A and Lewenstein M 1998 Volume of the set of separable states *Phys. Rev.* A **58** 883
[51] Vidal G and Werner R F 2002 Computable measure of entanglement *Phys. Rev.* A **65** 032314
[52] Kessler E M, Giedke G, Imamoglu A, Yelin S F, Lukin M D and Cirac J I 2012 Dissipative phase transition in a central spin system *Phys. Rev.* A **86** 012116
[53] Cai Z and Barthel T 2013 Algebraic versus exponential decoherence in dissipative many-particle systems *Phys. Rev. Lett.* **111** 150403
[54] Minganti F, Biella A, Bartolo N and Ciuti C 2018 Spectral theory of Liouvillians for dissipative phase transitions *Phys. Rev.* A **98** 042118
[55] Fitzpatrick M, Sundaresan N M, Li A C Y, Koch J and Houck A A 2017 Observation of a dissipative phase transition in a one-dimensional circuit QED lattice *Phys. Rev.* X **7** 011016
[56] Rodriguez S R K *et al* 2017 Probing a dissipative phase transition via dynamical optical hysteresis *Phys. Rev. Lett.* **118** 247402
[57] Fink T, Schade A, Hofling S, Schneider C and Imamoglu A 2018 Signatures of a dissipative phase transition in photon correlation measurements *Nat. Phys.* **14** 365
[58] Naghiloo M, Abbasi M, Joglekar Y N and Murch K W 2019 Quantum state tomography across the exceptional point in a single dissipative qubit *Nat. Phys.* **15** 1232
[59] Partanen M *et al* 2019 Exceptional points in tunable superconducting resonators *Phys. Rev.* B **100** 134505
[60] Chen W, Abbasi M, Joglekar Y N and Murch K W 2021 Quantum jumps in the non-Hermitian dynamics of a superconducting qubit *Phys. Rev. Lett.* **127** 140504
[61] Dogra S, Melnikov A A and Paraoanu G S 2021 Quantum simulation of parity–time symmetry breaking with a superconducting quantum processor *Commun. Phys.* **4** 26
[62] Chen W, Abbasi M, Ha B, Erdamar S, Joglekar Y N and Murch K W 2022 Decoherence induced exceptional points in a dissipative superconducting qubit *Phys. Rev. Lett.* **128** 110402
[63] Abbasi M, Chen W, Naghiloo M, Joglekar Y N and Murch K W 2022 Topological quantum state control through exceptional-point proximity *Phys. Rev. Lett.* **128** 160401
[64] Zhang J-W *et al* 2022 Dynamical control of quantum heat engines using exceptional points *Nat. Commun.* **13** 6225
[65] Bu J T *et al* 2023 Enhancement of quantum heat engine by encircling a Liouvillian exceptional point *Phys. Rev. Lett.* **130** 110402
[66] Han P-R *et al* 2022 $\mathcal{PT}$ symmetry and $\mathcal{PT}$-enhanced quantum sensing in a spin-boson system (arXiv:2210.04494v1)
[67] Han P *et al* 2022 Exceptional entanglement transition and natural-dissipation-enhanced quantum sensing (arXiv:2210.04494v2)
[68] Liang C, Tang Y, Xu A-N and Liu Y-C 2023 Observation of exceptional points in thermal atomic ensembles (arXiv:2304.06985)
[69] Li Z-Z, Chen W, Abbasi M, Murch K W, Whaley K B, Ozdemir S K, Zhou F, Jing H and Feng M 2022 Speeding up entanglement generation by proximity to higher-order exceptional points (arXiv:2210.05048)
[70] Quinn A, Metzner J, Muldoon J E, Moore I D, Brudney S, Das S, Allcock D T C and Joglekar Y N 2023 Observing super-quantum correlations across the exceptional point in a single, two-level trapped ion (arXiv:2304.12413)